IEEE Access
Multidisciplinary ⋮ Rapid Review ⋮ Open Access Journal

Received January 13, 2021, accepted February 19, 2021, date of publication March 1, 2021, date of current version March 9, 2021.

Digital Object Identifier 10.1109/ACCESS.2021.3062907

Feasibility Validation of a 5G-Enabled mmWave Vehicular Communication System on a Highway

GOSAN NOH, (Member, IEEE), JUNHYEONG KIM, (Member, IEEE), SEUNGNAM CHOI, NAMSUK LEE, HEESANG CHUNG, AND ILGYU KIM

Electronics and Telecommunications Research Institute (ETRI), Daejeon 34129, South Korea

Corresponding author: Gosan Noh (gsnoh@etri.re.kr)

This work was supported by the Institute of Information and Communication Technology Planning and Evaluation (IITP) grant funded by the Korea Government (MSIT), QoE improvement of open Wi-Fi on public transportation for the reduction of communication expense, under Grant 2018-0-00792.

ABSTRACT In this paper, we present an mmWave-based vehicle-to-infrastructure (V2I) communication system operating at a 22 − 23GHz frequency band, and evaluate its feasibility and effectiveness on an actual highway through a field trial. Based on a network layout that is well suited for the mmWave-based high mobility vehicular applications, we provide physical and higher layer design details, which are based on the 3GPP 5G New Radio (NR) standard. We then investigate key technologies to overcome the performance degradation of the mmWave-based system due to high mobility: a user equipment (UE)-oriented beam switching-based beamforming scheme, a fast and robust handover procedure with a two-step timing advance (TA) update, and mobile relaying for providing better quality-of-service (QoS) to in-vehicle UEs. The proposed system design and related key technologies are validated through a real-world testbed in an actual highway test site. Regarding this, we describe the specifics of testbed implementation and provide the experimental results obtained from the trial. The validation results show that the 5G NR-based mmWave system is feasible and effective for realizing high data rate vehicular communication on a highway.

INDEX TERMS 5G, high mobility, mmWave, testbed, vehicular communications.

I. INTRODUCTION

The advent of the fifth generation (5G) wireless technology has been facilitating much more advanced wireless networks in terms of data rate, reliability, latency, device density, and so on, across the three major 5G use cases: enhanced Mobile BroadBand (eMBB), Ultra-Reliable Low-Latency Communication (URLLC), and massive Machine-type Communication (mMTC) [1]. The above 5G use cases encompass various service verticals as well as traditional mobile services such as smartphones and tablets. One of such verticals is the vehicular applications which allow cars to be connected to the Internet, other cars, and pedestrians with the aid of the 5G network.

One aspect to be considered for the vehicular applications is the high mobility, i.e., the speed of cars driving on a highway can reach 140 km/h [2]. In this high mobility environment, system design should be done such that performance degradation due to the high Doppler can be minimized by optimizing the system parameters. Mobility-related functions, e.g., handover, need to be also improved.

In addition, 5G vehicular applications are expected to achieve quite high data rate in a high mobility environment. For example, several hundred Mbps of data rate per vehicle needs to be supported for video streaming or sensor information sharing [3]. In order to support such high data rate, supporting large bandwidth is essential. Due to the high mobility, high spectral efficiency techniques such as high order multiple-input-multiple-output (MIMO), which require accurate channel information feedback, are not feasible. As a result, it is desirable to employ mmWave frequency bands where a large chunk of contiguous spectrum can be easily obtained.

In this regard, a natural question arises: How well does the 5G-enabled mmWave vehicular communication system work in a high mobility (e.g., highway) environment? The objective of this paper is to answer to the above question by designing, implementing, and validating the 5G-based mmWave system on an actual highway environment.

The associate editor coordinating the review of this manuscript and approving it for publication was Li Zhang.

A. RELATED WORK

Mobility support has been a key component of wireless communication systems since the beginning of the cellular era. Mobility-related features such as time-varying channel estimation/tracking and handover have been considered important to provide acceptable service quality while a mobile device is in motion. This tendency continued to the latest generation, namely 5G mobile communication. In 3GPP 5G New Radio (NR), further advancements regarding high mobility were made including support for the larger subcarrier spacing (or equivalently shorter orthogonal frequency-division multiplexing (OFDM) symbol period), dense reference signal allocation in the time domain, the introduction of new reference signal dedicated to the time/frequency tracking, more robust and seamless handover schemes such as conditional handover and dual active protocol stacks (DAPS), and so on [4]–[6].

Thanks to these features, 5G NR systems are able to better satisfy the link performance across diverse speed requirements up to 500 km/h [7]. This is in contrast to the previous 4G LTE, which is best optimized to the zero-to-low mobility user equipments (UEs) (from 0 km/h to 15 km/h) while providing less optimized services to the higher mobility UEs, i.e., providing high performance services to mid-mobility UEs (from 15 km/h to 120 km/h) and functional services to high-mobility UEs (from 120 km/h to 350 km/h) [8].

With the successful development of 5G NR standard, the commercial deployment of 5G NR is now being conducted worldwide. However, in most countries, lower frequency bands, namely Frequency Range 1 (FR1) (from 0.41 GHz to 7.125 GHz) dominate over the mmWave bands, namely FR2 (from 24.25 GHz to 52.6 GHz). Up to now, the deployment of mmWave bands is limited only to the applications with zero or low mobility such as backhauling, indoor access, etc [9], [10].

Although mass deployment of mmWave is yet to come, considerable research efforts on the high-mobility mmWave-based wireless communications are currently underway in the areas of channel measurement and modeling, modulation/detection, channel estimation/tracking, beam management, and handover.

A Doppler measurement for the 28 GHz vehicle-to-infrastructure (V2I) channel was performed in an actual highway in [5], which revealed the effects of moving and static objects on the Doppler shift. Ray tracing-based channel modeling was conducted for the mmWave V2I link in [11], which evaluated various channel properties including Rician K-factor, delay spreads, angular spreads, etc. In [12], the diffraction loss in an over-rooftop propagation environment at a mmWave frequency band was measured and compared with the knife-edge diffraction (KED) and geometrical theory of diffraction (GTD) models.

A new modulation and detection technique, namely single-carrier modulation with time-domain equalization (SC-TDE) and frequency-domain multiplexing with a frequency-domain cyclic prefix (FDM-FDCP), was proposed in [13], which showed significant performance improvements in high-mobility and mmWave channels. In [14], it was shown that employing orthogonal time-frequency space (OTFS) modulation is robust to phase noise in high Doppler mmWave channels. In [15], a generalized spatial modulation scheme was proposed for high mobility mmWave systems, which relies on a large-scale differential detection.

An exploitation of sparsity in a frequency-selective mmWave channel was proposed for channel estimation in high mobility scenarios [16]. A time-varying channel estimation scheme was proposed for mmWave multiuser MIMO systems in [17], which exploited the property that the arrival and departure angles vary much slower than the path gains. A Doppler shift estimation algorithm was proposed using a newly designed training sequence for mmWave vehicular communication systems [18].

In [19], a joint beam direction and channel coefficient tracking algorithm was developed to achieve reliable mmWave connectivity for fast-moving mobiles. An adaptive beamwidth control scheme was proposed in [20], which can improve mmWave beam tracking performance in a high mobility environment.

A dual connectivity-based handover protocol which can overcome the effect of blockage occurring in mmWave mobile networks was proposed [21]. In [22], a handover decision strategy for mmWave cellular networks based on a Markov decision process framework was proposed.

B. CONTRIBUTIONS AND ORGANIZATION

As discussed above, there have been a lot of existing works on mmWave vehicular communication. However, the outcomes from these works are not sufficient to fully understand whether the use of mmWave frequency bands is valid and useful in the high mobility scenario since they are mostly theoretical solutions. Hence, as a next step, it is necessary to develop a real-world testbed and conduct a field test in an appropriate vehicular environment. Hence, in this paper, we develop and evaluate a 5G NR-based mmWave vehicular communication testbed in a highway V2I scenario. More specifically, based on a network layout well suited for the highway environment, we provide the 5G NR system design details including physical layer (i.e., Layer-1 (L1)) and higher layers (i.e. Layer-2 (L2) and Layer-3 (L3)) with emphases on the use of mmWave frequency bands and high mobility. We further investigate key technologies necessary for supporting the mmWave-based system operating in a high mobility scenario, including a UE-oriented beam switching scheme, a handover procedure with a two-step timing advance (TA) update, and mobile relaying for in-vehicle UEs. We then describe the mmWave testbed implementations both of the gNodeB and UE. Based on the implementation, we provide the deployment details on an actual highway test site and the obtained experimental results such as signal-to-noise ratio (SNR), data rate, etc.

This organization of this paper is as follows. A system design description including network layout, physical layer overview, and higher protocol processing is provided in Section II. Key technologies to better support high mobility

in a mmWave system is discussed in Section III. Details of testbed implementation, deployment, and validation through field testing are provided in Section IV. Finally, Section V concludes the paper.

II. SYSTEM DESIGN

In this section, we describe the design details of the employed 5G NR-based mmWave vehicular communication system. Based on a network layout description, a physical layer overview is provided, followed by a brief summarization of L2 and L3 protocol processing.

A. NETWORK LAYOUT

A network layout describing an mmWave vehicular communication system on a highway is illustrated in Fig. 1. A gNodeB consists of one or more central units (CUs) and one or more distributed units (DUs). The gNodeB functions are split into the CU and DU according to Option 6 (i.e., MAC-PHY split) among the 3GPP Radio Access Network (RAN) split options[1] [23], which means that higher layer protocols are processed in the CU, and physical layer and RF front-end are placed in the DU. The DUs are installed on roadside locations. The fronthaul connection between the CU and DU is based on optical fiber, which can facilitate, for example, centralized scheduling and traffic load management requiring tight timing interactions between CU and DUs [24].

Vehicle UEs are equipped on cars driving on a highway at high speed. By establishing wireless connectivity to the gNodeB, the vehicle UE can serve to satisfy diverse vehicular communication requirements. One promising usage is the Tethering-via-Vehicle use case where a vehicle UE acts as a mobile relay to provide wireless connectivity to in-vehicle UEs such as passengers [3], [25]. In this use case, a large amount of data rate is expected to be supported.

For the carrier frequency band, an mmWave frequency band around $22-23$ GHz is employed to achieve Gbps data transmission thanks to the abundant bandwidth availability. In order to overcome higher path loss and higher susceptibility to the blockage inherent to mmWave bands [26], beamforming is employed both at the DU and vehicle UE. From the DU side, a high-gain narrow beam is generated so as to cover the road area. This is particularly suited to the highway environment where the road tends to be straight or only slightly curved. A uni-directional beamforming, where beams from DUs see the same direction (i.e., the opposite of the driving direction), is assumed for each DU. This enables an almost constant Doppler shift, making the Doppler compensation much easier. The vehicle UE is further equipped with a beam selection capability so as to maintain the best beam pair with its serving DU. This is particularly useful when the vehicle changes its driving direction, e.g., changing lanes or passing other vehicles, as to be further discussed in Section III-A.

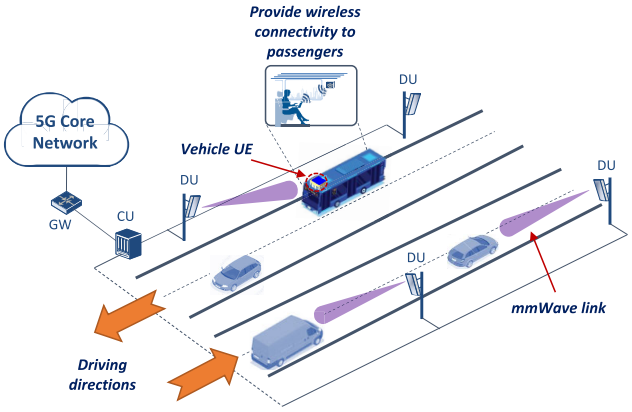

FIGURE 1. Network layout.

B. PHYSICAL LAYER OVERVIEW

The physical layer of the proposed system is largely based on the 5G NR specifications but the specific configuration is tailored to the mmWave high mobility usage. The 5G NR supports flexible numerology with scalable subcarrier spacing (SCS) so as to be fitted for the various frequency bands and deployment scenarios. Since the proposed system is implemented to operate around the $22-23$ GHz band, which is quite close to the lower bound of FR2, the SCS values of 60 kHz and 120 kHz (or equivalently $\mu = 2$ and $\mu = 3$) are supported for the data channels (i.e., physical downlink shared channel (PDSCH) and physical uplink shared channel (PUSCH)) and control channels (i.e., physical downlink control channel (PDCCH) and physical uplink control channel (PUCCH)) in the downlink and uplink directions respectively, which are sufficient to combat against severe phase noise and Doppler spread occurred in the mmWave system.

Since a vast amount of spectrum is available in the $22-23$ GHz band that is utilized for the link between the DU and vehicle UE, the proposed system is designed to support carrier aggregation (CA) that allows each gNodeB to aggregate up to six component carriers (CCs), each of which having a bandwidth of 100 MHz, so as to achieve the total transmission bandwidth of up to 600 MHz.

An exemplary frame structure of the proposed system is depicted in Fig. 2. A radio frame with 10 ms duration consists of ten subframes with each subframe having 1 ms duration. Since the SCS of 60 kHz is selected for the data transmission in this example, each subframe is divided into four slots. Therefore, there are a total of 40 slots in one radio frame, and the slots within a frame are numbered from 0 to 39. A slot is a basic scheduling granularity and consists of 14 OFDM symbols. As seen in Fig. 2, it is chosen in this paper that, for the time division duplex (TDD) configuration, within one radio frame, every slot is used for the downlink transmission except for the 7-th, 15-th, 23-th, 31-th, and 39-th slots that

[1]Supporting various split options enables implementation flexibility in different deployment scenarios. Splitting in higher layers, e.g., Options 1-3, is best suited for low latency applications while splitting in low layers, e.g., Options 7 and 8, facilitates joint processing such as coordinated multi point (CoMP).

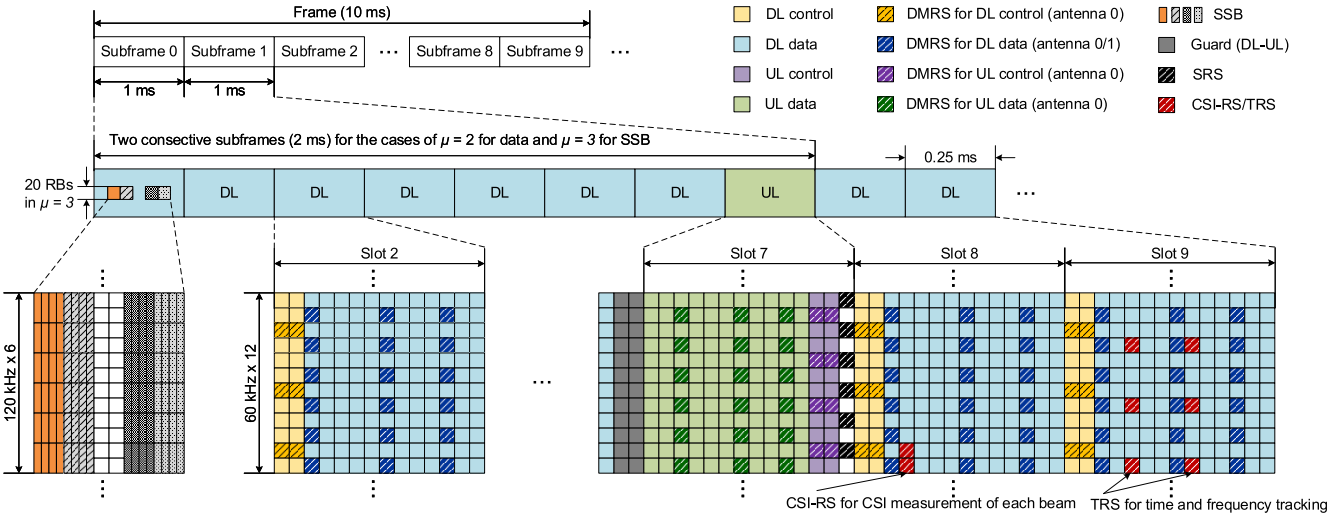

FIGURE 2. Frame structure.

are used for the uplink transmission. The last two symbols of the downlink slot just before each uplink slot are reserved for guard period (GP) to avoid overlap between the downlink and uplink transmissions considering the round trip time (RTT) and RF switching time from downlink to uplink and vice versa.

The vehicle UE performs cell search by receiving and detecting a synchronization signal block (SSB) from the gNodeB. The SSB consists of a primary synchronization signal (PSS), a secondary synchronization signal (SSS), and a physical broadcast channel (PBCH). The SCS of the SSB is selected to be 120 kHz. Hence, each resource element of the SSB is twice larger than that of the data channels in the frequency domain but is half in the time domain. As depicted in Fig. 2, an SSB burst set in slot 0 of each radio frame contains four SSB resources. Among them, one SSB is selected by the gNodeB and is transmitted with a period of 10 ms. At the same time, the gNodeB allocates no data to the remaining SSB resources. The rationale behind this design is to prevent the SSB from overlapping with the SSBs transmitted from other gNodeBs, by assigning the SSBs from different gNodeBs to different SSB resources within the SSB burst, which is particularly effective in performing neighbor cell search for handover [27].

Considering high mobility nature of the vehicle UE, MIMO transmission up to two layers is supported since higher MIMO multiplexing gain is very limited due to, for example, outdated channel state information (CSI). Since the line-of-sight (LOS) component dominates over the non-LOS (NLOS) components in the mmWave channel, polarization multiplexing is employed for the discrimination between the two antenna ports [28]. In this regard, a demodulation reference signal (DM-RS) with two antenna ports is employed. As seen in Fig. 2, in the frequency domain, the DM-RS can be allocated according to the DM-RS Configuration Type 1 (i.e., Comb-type) and the two DM-RS ports (i.e., port 0 and port 1) can be multiplexed in a code-division multiplexing (CDM) manner [29]. In the time domain, three DM-RS symbols can be allocated within a slot in order to improve channel estimation performance in the high mobility scenario.

CSI-RS is used in the downlink for diverse purposes: downlink CSI acquisition, time/frequency tracking, etc. The CSI-RS is configured to be transmitted in slot 8 and slot 9 for every radio frame. The CSI-RS in slot 8 is mainly used for downlink CSI estimation and RSRP measurement for an automatic gain control (AGC) operation, while the CSI-RS in slot 9, also known as tracking RS (TRS), is mainly responsible for time and frequency tracking in an automatic frequency control (AFC) operation.

For the random access procedure, the vehicle UE transmits a preamble for the physical random access channel (PRACH). The PRACH preamble format C2, a short sequence preamble format with the preamble length of 139, is used, and the SCS of the preamble is chosen as 60 kHz in order to ensure an appropriate cell coverage for the highway scenario. The number of PRACH occasions in the frequency domain is configured as one, and the number of time occasions per PRACH slot is configured as two. Since the five uplink slots can be used for PRACH transmissions within a 10 ms radio frame, there are a total of ten PRACH ocassions, each of which is associated with the corresponding SSB.

A sounding reference signal (SRS) is mainly used for the uplink channel sounding and can be further used for the uplink timing estimation at the gNodeB. The SRS is allocated in a Comb-2 fashion in the frequency domain. Considering high mobility nature, the SRS is transmitted in the last symbol of every uplink slot, i.e., every 8-th slot.

The detailed physical layer parameters are summarized both for the 60 kHz (i.e., $\mu = 2$) and 120 kHz (i.e., $\mu = 3$) SCS values in Table 1.

TABLE 1. Physical layer parameters.

Parameters	$\mu = 2$	$\mu = 3$
Carrier frequency (GHz)	22.6	22.6
Subcarrier spacing (kHz)	60	120
Sampling rate (MHz)	122.88	122.88
System bandwidth of each CC (MHz)	100	100
Fast Fourier Transform (FFT) size	2048	1024
Number of physical resource blocks (PRBs)	132	66
Number of subcarriers per RB	12	12
Number of slots per subframe	4	8
Slot duration (μs)	250	125
Number of OFDM symbols per slot	14	14
Cyclic prefix (CP) duration (μs)	1.17	0.57
OFDM symbol duration w/o CP (μs)	16.67	8.33
OFDM symbol duration w/ CP (μs)	17.84	8.92

C. L2/L3 PROTOCOL PROCESSING

L2/L3 layer protocols are responsible for handling the user plane and control plane procedures on top of the physical layer. The proposed system implements all the 5G NR L2/L3 protocol stacks. The functionality of each sub-layer protocol within the L2/L3 layer is briefly summarized below [30]:

- **Service Data Application Protocol (SDAP)** maps between QoS flows and radio bearers based on the QoS requirement of each QoS flow.
- **Packet Data Convergence Protocol (PDCP)** is responsible for header compression/decompression, ciphering/deciphering, integrity protection/verification, in-order delivery, duplicate discarding, etc.
- **Radio-Link Control (RLC)** is required to support one of three transmission modes: transparent mode (TM), unacknowledged mode (UM), and acknowledged mode (AM). Depending on the transmission mode, RLC performs automatic repeat request (ARQ), segmentation/resegmentation, duplicate detection, and so on.
- **Medium-Access Control (MAC)** sublayer manages multiplexing/demultiplexing between logical channels and transport channels, hybrid ARQ (HARQ) operation, and scheduling.
- **Radio Resource Control (RRC)** manages several control-plane operations including system information broadcasting, paging, RRC connection establishment/release, radio bearer management, mobility functions including handover and cell reselection, UE measurement, radio link failure (RLF) management, and so on. RRC can be one of the three states: **RRC_IDLE**, **RRC_INACTIVE**, and **RRC_ CONNECTED** depending on the activity of a UE, i.e., unicast data transfer of the UE is only possible for the **RRC_ CONNECTED** state. If the UE expects no data transfer in the near future, it transits to the **RRC_IDLE** or **RRC_INACTIVE** state.

The proposed mmWave vehicular communication system is required to support Gbps data transmission while tackling problems due to very high carrier frequency and high mobility. Hence, several considerations related to the high mobility support need to be taken into account for the L2/L3 layer protocol operations. Regarding this, one important function is to obtain and maintain uplink synchronization since the uplink timing can be rapidly varying due to higher UE mobility. For the initial uplink synchronization, a typical four-step random access procedure is performed, which is controlled both by L2 and L3. The first step is the transmission of the PRACH preamble from the UE to the gNodeB as described in Section II-B. Then, after correlating the received PRACH preamble with a set of reference preambles, the gNodeB calculates the amount of uplink timing delay of the UE. Once the gNodeB detects the preamble, it informs the vehicle UE of the reception of the preamble and provides a TA command by sending a random access response (RAR) message. Then, the UE adjusts its uplink timing according to the TA command within the RAR message. If this uplink timing is appropriate, the random access procedure will be completed by successfully exchanging the connection request (Msg3) and contention resolution (Msg4) messages between the UE and gNodeB.

As vehicle UEs generally travel at high speeds on a highway, it is necessary for the vehicle UE to periodically update uplink transmission timing to better align with the frame timing at the network side. Therefore, the gNodeB keeps estimating the uplink timing difference using the SRS and sends back the corresponding TA command to the vehicle UE through a MAC control element (MAC CE).

III. KEY TECHNOLOGIES FOR MMWAVE HIGH MOBILITY SUPPORT

This section discusses the key technologies essential for overcoming the performance degradation due to high mobility in a mmWave system, which include beamforming, handover, and mobile relaying.

A. BEAMFORMING

Beamforming is one of the key components to provide proper coverage and better link quality of mmWave-based systems, by which the desired signal is concentrated to a preferred direction. By doing so, the following favorable effects of beamforming are observed: increased signal power, reduced power consumption, reduced interference level, etc. Narrowing beamwidth by beamforming also reduces the Doppler spread, by which severe link performance degradation, e.g., inter-carrier interference (ICI), can be alleviated in the high mobility scenario [31].

Continuing the above principle, from the gNodeB side, it is natural to generate a beam along the highway road since cars drive in the same direction within the road area. In this situation, employing a fixed beam facing towards the opposite of the road travel direction will be a good option to provide

enough coverage area and acceptable link quality, as seen in Fig. 3.

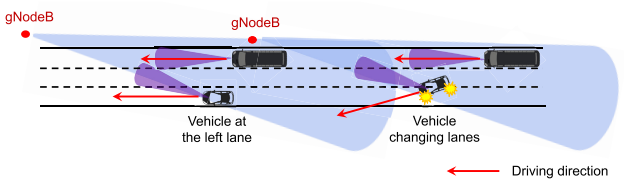

FIGURE 3. Beamforming operations.

Oppositely, from the vehicle UE side, supporting beam switching (or beam steering) capability can provide a significant performance gain. For example, it will be beneficial to use the beam pointing to the right-hand side of the vehicle for the vehicles at the left lanes or those changing the lane to the left, as also seen in Fig. 3.

Hence, in the proposed system, a UE-centric beam switching operation is employed, i.e, beam switching is performed only at the vehicle UE. In addition, a beam correspondence property between the transmit and receive beams at the vehicle UE is utilized [4]. Thus, the uplink beam selection is done based on the downlink beam measurement, so as to minimize the signaling overhead and network operation burden for the beam management operation. For the beam measurement, an SSB is used to measure the received beam power (i.e., RSRP). The periodicity of the SSB is configured as 10 ms to enable frequent beam measurements. The measured RSRP is then averaged for each beam over the 240 ms window, which corresponds to the travel distance of 6.67 m for a vehicle driving at 100 km/h. By comparing the average RSRP among the receive beams, the best beam with the highest average RSRP is selected for transmitting and receiving signals at the vehicle UE.

B. HANDOVER

A handover procedure is typically triggered based on the RSRP measurement at the UE. Upon the measurement request message from the serving gNodeB (S-gNB), the UE measures the RSRP of the target gNodeB (T-gNB) as well as that of the S-gNB. The measured RSRPs are further averaged (i.e., L3 filtering) and then are reported to the S-gNB. Fig. 4 shows the RSRP distributions of the S-gNB and T-gNB as time elapses during the handover operation. In the conventional handover situation where the beam of each gNodeB is omni- or bi-directional, the RSRP of the S-gNB gradually decreases while that of the T-gNB gradually increases at the cell boundary as seen in Fig. 4a. When the RSRP of the T-gNB becomes higher than that of the S-gNB by an offset (i.e., a positive offset is used in this case to avoid the ping pong effect), an A3 event occurs and the handover is triggered [32]. The triggering condition for the A3 event can also be expressed as

$$Mn + Ofn + Ocn - Hys > Mp + Ofp + Ocp + Off, \quad (1)$$

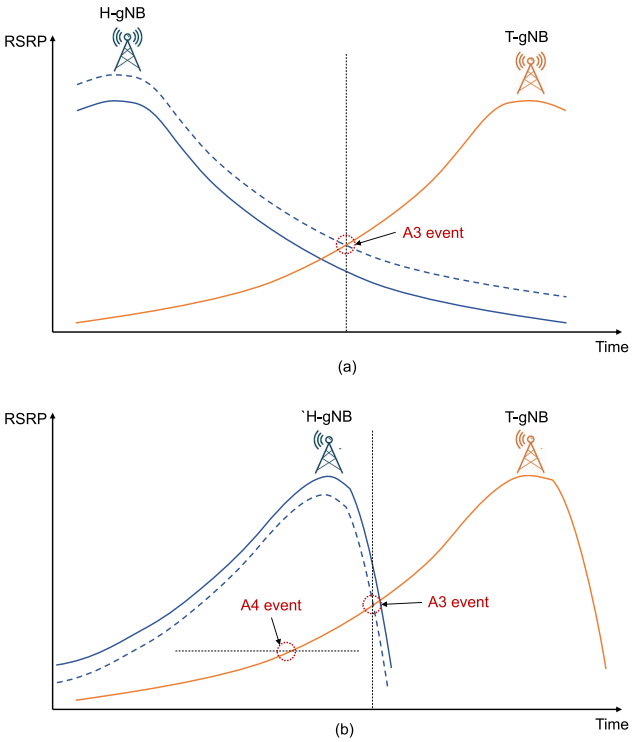

FIGURE 4. RSRP distribution during handover: a) Conventional omni- or bi-directional gNodeB deployment; b) Uni-directional gNodeB deployment.

where Mn and Mp are the RSRP measurement results of the T-gNB and S-gNB, respectively. Ofn and Ofp are the measurement specific offset values of the T-gNB and S-gNB, respectively. Ocn and Ocp are the cell specific offset values of the T-gNB and S-gNB, respectively. Hys and Off are the hysteresis parameter and offset parameter for the event, respectively, which are used to reduce the ping pong effect [33].

Oppositely, when the beam of each gNodeB is unidirectional, i.e., the beam of every gNodeB points to the opposite to the driving direction of the highway, the RSRP of the S-gNB abruptly decreases while that of the T-gNB gradually increases at the cell boundary as seen in Fig. 4b. In this case, there will not be enough time to trigger, execute, and complete handover before the signal from the S-gNB is lost, thereby increasing handover failure rate.

In order to avoid such a handover failure situation, the handover operation needs to be prepared earlier. Hence, we use an A4 event in addition to the A3 event as seen in Fig. 4b. The A4 event is triggered when the RSRP of the T-gNB is higher than a predefined threshold, or equivalently:

$$Mn + Ofn + Ocn - Hys > Thresh, \quad (2)$$

where $Thresh$ is the threshold parameter for the event [32].

If the UE identifies the A4 event, a handover preparation operation is started by notifying the A4 event to the S-gNB. Then, the S-gNB sends the handover request message to the T-gNB. Upon the reception of the acknowledgement from the T-gNB, the S-gNB sends the handover command

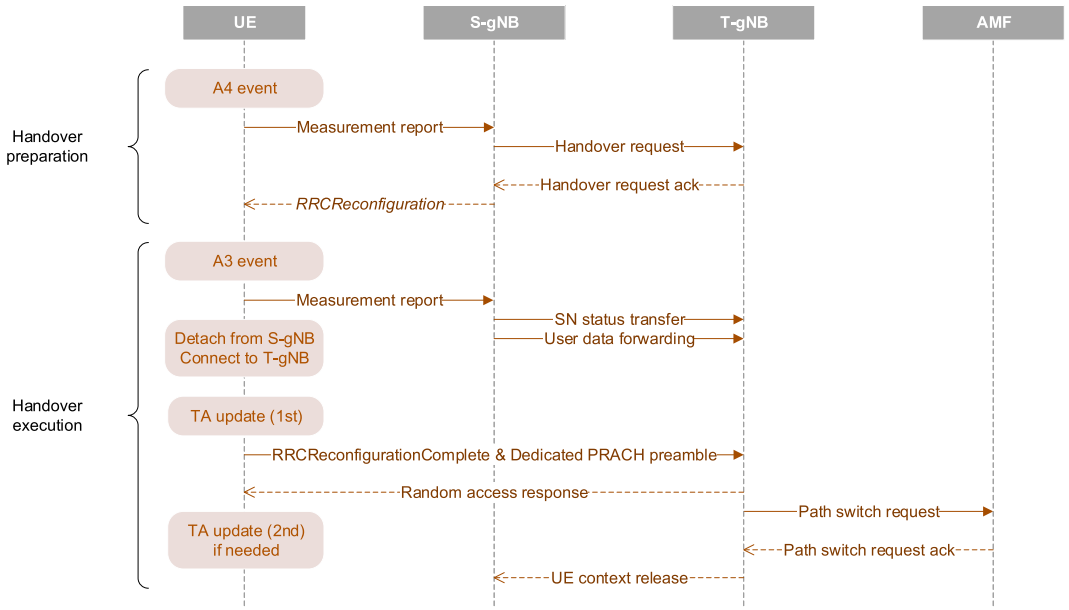

FIGURE 5. Handover procedure.

(i.e., *RRCReconfiguration* message) to the UE so that the UE becomes ready for handover. After the A4 event occurs and then the UE further moves to the T-gNB, the A3 event occurs (a negative offset is selected in this case to enable faster handover before the connection with the S-gNB is lost), thereby triggering handover execution. Then, the sequence number (SN) status and user data are forwarded to the T-gNB.

Meanwhile, the UE needs to prepare to attach to the T-gNB. Here, one of the most important such tasks is to obtain uplink synchronization with the T-gNB by updating the TA value. In order to minimize handover latency while not increasing the handover failure rate, we propose a two-step TA update mechanism, where the TA can be updated before and after the random access procedure. More specifically, the first TA update is done by calculating the TA value for the T-gNB, TA_t, based on the propagation delay difference between the S-gNB and T-gNB, similar to the RACH-less handover [34]. Assuming that the S-gNB and T-gNB are synchronized, TA_t can be expressed as

$$TA_t = TA_s - 2(D_s - D_t), \tag{3}$$

where TA_s is the TA value for the S-gNB. D_s and D_t are the propagation delay measured in the downlink for the S-gNB and T-gNB, respectively.

Using the updated TA value, the UE sends *RRCReconfigurationComplete* message and the dedicated PRACH preamble to the T-gNB.[2] If the above calculated TA value is accurate, the T-gNB will successfully receive the *RRCReconfigurationComplete* message and there will be no need for the second TA update, significantly reducing the handover latency. Otherwise, after the random access procedure, the second TA update is performed as per indicated in the RAR, which can yield longer handover latency but can overcome the handover failure due to inaccurate TA value estimation that can sometimes be unavoidable in the high mobility scenario. In this case, *RRCReconfigurationComplete* message will be retransmitted.

Upon the reception of the *RRCReconfigurationComplete* message, the T-gNB exchanges the path switch request and its acknowledgement with the Access and Mobility Management Function (AMF). Then, the T-gNB sends the UE context release message to the S-gNB, completing the handover procedure. The entire handover procedure including both the preparation and execution phases is summarized in Fig. 5.

C. MOBILE RELAYING

Due to the higher sensitivity to the blockage and severe shadowing of the mmWave frequency band, relying only on the direct link between the gNodeB and UE will not be sufficient to guarantee QoS requirements. In a highway environment, various objects can be considered as obstacles for the link between the gNodeB and in-vehicle UEs.

For the in-vehicle UEs, the most dominant factor of such a blockage is the penetration loss caused by a vehicle body made of metallic material [8]. As seen in Fig. 6, such high penetration loss can be avoided through an onboard relay installed on a vehicle. The backhaul part and access part of the onboard relay can be separately installed outside and inside of the vehicle to support the backhaul link to the gNodeB and the access link to the in-vehicle UE, respectively. In addition, thanks to the reduced link distance, the power consumption of the in-vehicle UEs which are typically battery-operated is also greatly reduced. Another advantage of employing a

[2]The two uplink messages do not have to be transmitted at the same time. The transmission times depend on the uplink availability and message preparation.

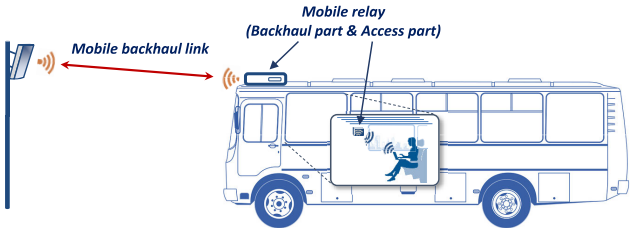

FIGURE 6. Mobile relaying operation. Mobile relay is deployed on the outside (backhaul part) and inside (access part) of a vehicle.

mobile relay is more alleviated restrictions on power consumption, form factor, etc. of the onboard relay deployed on a vehicle. Hence, more powerful and advanced techniques can be used in the baseband modem, RF circuitry, and antenna, thereby providing more robust and efficient connectivity with the gNodeB.

The implementation of the access link between the vehicle onboard relay and the in-vehicle UEs can be done using, for example, a small cell or WiFi technology. In this case, supporting the access link within the vehicle is done independently from the backhaul link (i.e., the link between the gNodeB and vehicle UE), enabling wireless access to the in-vehicle UEs (e.g., passengers) without any UE modifications. This kind of service scenario can be best suited to the WiFi access in the public transportation like buses.

IV. TESTBED IMPLEMENTATION, DEPLOYMENT, AND VALIDATION ON THE HIGHWAY TEST SITE

In this section, we describe the system implementation aspects both for the gNodeB and UE. We then specify the actual deployment of the implemented system on a highway for validation. We also provide the field trial results including SNR distribution, data rate, etc.

A. CU AND DU IMPLEMENTATIONS

As seen in Fig. 7 and described in Section II-A, the gNodeB consists of the CU and DU, where L2/L3 functionalities are performed in the CU and the L1/RF modules are implemented in the DU, respectively. The CU is connected to the 5G Core, which is further connected to the Internet. For improved flexibility, all the L2/L3 protocol stacks are implemented by software on a 2.6 GHz Intel XEON processor (E5-2697A v4).

The L1 baseband processing is done in the baseband board of the DU. Time-ciritical physical layer functionalities are implemented using three Xilinx Kintex UltraScale field-programmable gate arrays (FPGAs) (XCKU115-FLVB1760). Among the three FPGAs, one FPGA is responsible for transmitting/receiving packets (e.g., transport block data) to/from L2 and L3, controlling modem timer, managing synchronization operation, and so on. The other two FPGAs are dedicated for the physical layer processing including channel encoding/decoding, scrambling/descrambling, modulation/demodulation, MIMO precoding/combining, resource mapping/demapping, etc. TI DAC38RF80 and TI ADC32RF45 are employed for the digital-to-analog (DA) and analog-to-digital (AD) converters, respectively. These baseband modules are controlled by the L1 controller, which is implemented by software on a STM32H743I processor.

The RF module can process wideband RF signals with a bandwidth of 600 MHz at a center frequency of 22.6GHz. The TDD switching time is up to 5 μs. In order to support 2×2 MIMO transmission, two different RF paths are equipped both for the transmit and receive RF paths. For the transmit RF path, the maximum RF transmit power is 17 dBm. It was measured that the error vector magnitude (EVM) is 2.5% and the adjacent channel leakage ratio (ACLR) is 40 dBc, respectively. For the receive RF path, a noise figure of 5 dB is achieved.

As seen in Fig. 7, a slotted array waveguide antenna having 4×4 radiating slots is employed, which can provide high power efficiency, low power loss, and high stability [35]. For both the transmit and receive paths, two array antennas are deployed in a dual-polarized manner (i.e., one in the vertical direction and the other in the horizontal direction), so that they can be used for MIMO transmission and reception. From the measurement for the implemented antenna, transmit/receive antenna array gain is 19 dBi and the half-power beamwidth is 18°.

The interconnection between the CU and DU (i.e., fronthaul) is based on 10G Ethernet over fiber. In order to connect a large number of pairs of CU and DU while using a single optical fiber core, a dense wavelength-division multiplexing (DWDM) scheme is employed [36].

Synchronization among the DUs can be realized using a synchronization unit, which is also connected to the DUs in a DWDM manner. The synchronization unit can enable the DUs to acquire clock- and frame-level synchronization by providing 10 MHz reference clock and pulse per second (PPS), both of which enable the DUs to be synchronized when transmitting signals. The mismatch due to the difference of the optical fiber lengths is also compensated at each DU. By doing so, the TA update can be done before the random access procedure during the handover operation, thereby significantly reducing the handover latency as discussed in Section III-B.

B. VEHICLE UE IMPLEMENTATION

As seen in Fig. 7, L1/RF and L2/L3 functionalities of the vehicle UE are performed in separate modules. Similar to the gNodeB, the UE L2/L3 protocol stacks are implemented by software on a 2.2 GHz Intel XEON processor (D-2183IT). Since the same baseband board is shared by both the DU and vehicle UE, the UE L1 functionalities are implemented on the FPGA chips, similar to the DU.

The main differences of the vehicle UE from the gNodeB-DU are the RF and antenna parts. As described in III-A, the vehicle UE has a beam switching capability. To do so, the vehicle UE has three transmit and receive array antenna pairs, each of which consists of vertically and

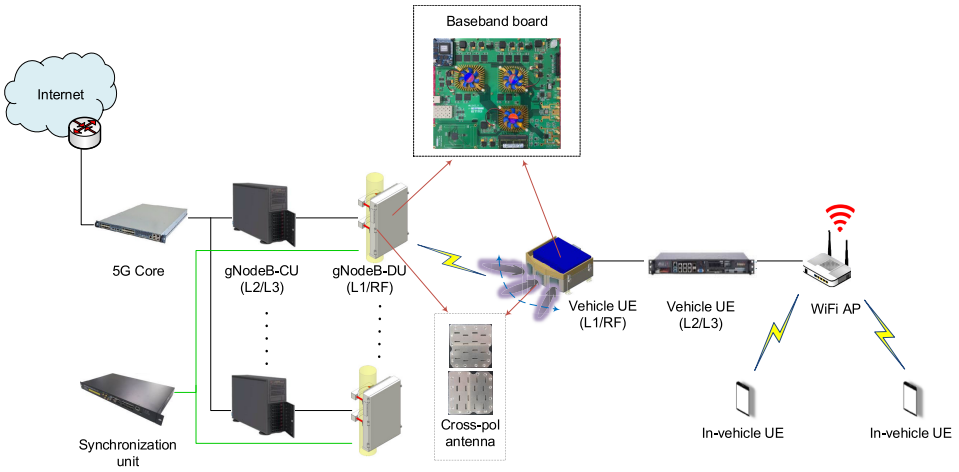

FIGURE 7. Implementation overview.

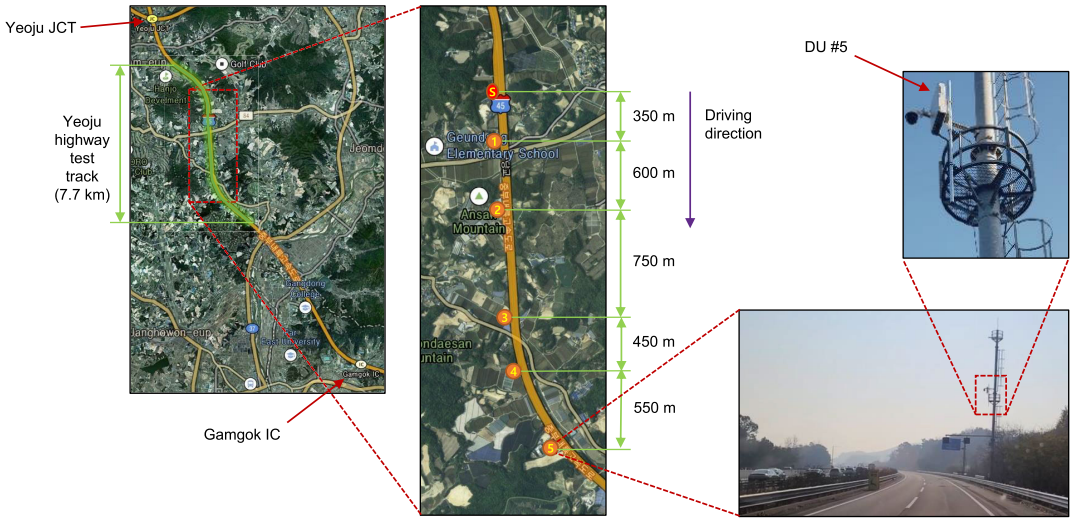

FIGURE 8. DU deployment on a highway test track.

horizontally polarized components. The beam switching is controlled by L1 controller based on the RSRP measurements. The beam switching time is measured less than 1 μs.

In-vehicle UEs (e.g., smartphones) can access the network through a WiFi access point (AP) installed inside the vehicle, which is universally available and has a small coverage within a vehicle.

C. DEPLOYMENT FOR A HIGHWAY FIELD TRIAL

The implemented DUs are deployed on a highway test track for the field trial. The test track is located between Yeoju junction (JCT) and Gamgok interchange (IC) of Highway 45 of Korea, which was built parallel to the main highway. Out of total 7.7 km test track, a section of 2.7 km is actually used for the trial, where 5 DUs are deployed along the test track as illustrated in Fig. 8. The DUs are marked from "1" to "5" and the starting position of the vehicle is marked "S". The distance between the consecutive DUs is from 450 m to 750m. Each DU is mounted on a road side steel pole 15 m above the ground. Two cores of optical fibers are connected to each DU: One for the fronthaul connection to the CU and the other for the synchronized operation among the DUs.

Fig. 9 shows the test vehicle moving towards the DU. It can be observed that the DU is installed such that the beam of the DU sees the front face of the vehicle and the beam of the vehicle UE sees the driving direction of the vehicle. In addition, equipped with a beam switching capability, the vehicle UE can select the best beam among the three beams. The angular difference between the directions of the consecutive beams is 15°, so that the vehicle UE can cover around 48° in total. For each beam direction, two 4 × 4 antenna arrays are placed and they are orthogonally polarized each other (i.e., horizontal polarization (H-pol) and vertical polarization (V-pol)), enabling 2 × 2 MIMO operation. The overall vehicle

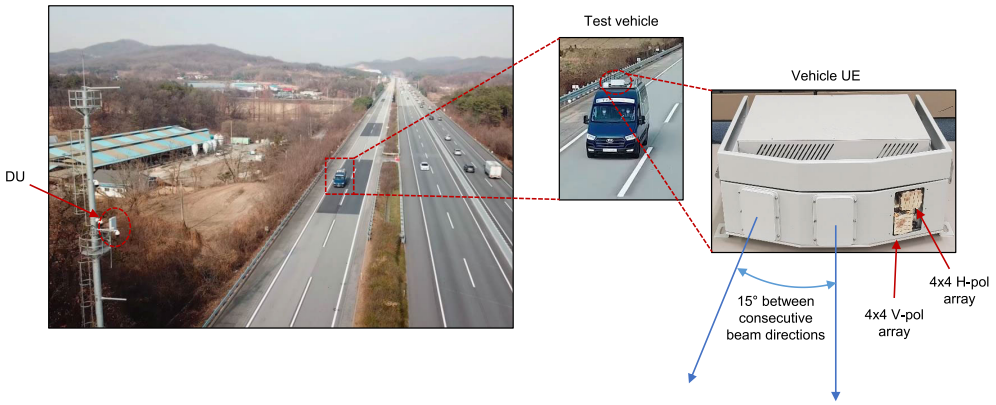

FIGURE 9. Test vehicle and vehicle UE.

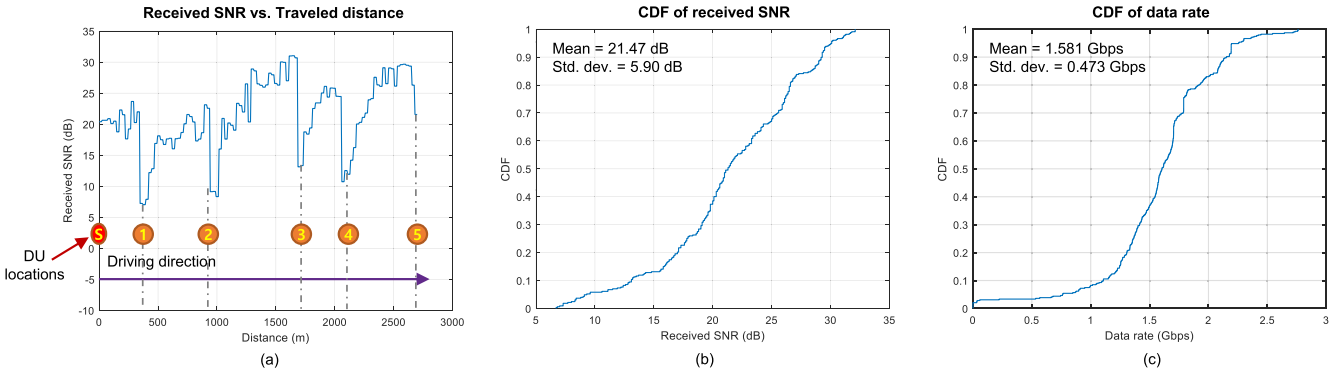

FIGURE 10. Field trial results: a) Received SNR vs. traveled distance; b) CDF of received SNR; c) CDF of data rate.

UE dimension is approximately 500 × 460 × 230 mm (W × L × H).

D. FIELD TRIAL RESULTS

The results of the field trial conducted on the highway test track are provided in Fig. 10, which show the received SNR along with the traveled distance (Fig. 10a), the cumulative distribution function (CDF) of received SNR (Fig. 10b), and the CDF of data rate (Fig. 10c).

Fig. 10a shows the received SNR as the test vehicle moves along the path from "S" (starting position) to "5" (last DU). The measured SNR ranges from 7 dB to 30 dB. It can be seen that the measured SNR is decreased with the distance between the DU and vehicle, obviously due to the increased path loss. In addition, the SNR is further decreased in the cell boundary regions, due to the interference from the neighboring DU. The CDF of the measured SNR is depicted in Fig. 10b.

Fig. 10c depicts the CDF of the measured data rate at the vehicle UE. Employing an adaptive modulation and coding (AMC) scheme along with the channel quality information (CQI) feedback, a set of modulation order (from QPSK to 64QAM) and code rate (from 0.245 to 0.889) is adaptively selected. As a result, it is seen that the measured data rate is closely related to the received SNR. It can also be observed that at least 1.15 Gbps of data rate is achievable for the 90% of the time during the test.

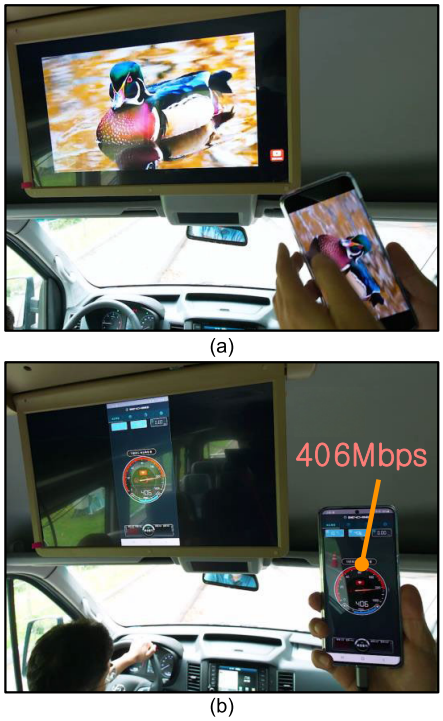

FIGURE 11. Field trial results: a) Video streaming test; b) Benchmark test.

Fig. 11 shows the video streaming test (in Fig. 11a) and benchmark test (in Fig. 11b), which were done using

a Samsung Galaxy S20 smartphone in order to assess the passenger quality of experience. During the test, only WiFi connection to the in-vehicle access point (AP) (Netgear Nighthawk AX12) was activated while the LTE/5G network connections were turned off. The in-vehicle AP was provided the Internet connection through the vehicle UE. In the video streaming test, 1080p (full HD quality) YouTube video was played without any interruption. In the benchmark test, BenchBee speed test application was used to measure the data rate achievable by the smartphone. Although upper bounded by the WiFi connection capacity, around 400 Mbps data rate was measured by a smartphone. Hence, it is expected to support up to 7 or 8 such WiFi connections at the same time.

V. CONCLUSION

In this paper, we investigated whether a 5G-enabled mmWave V2I communication system is feasible and useful by designing, implementing, and evaluating a real-world testbed in an actual highway environment. Based on a vehicular network layout specifically tailored to a highway environment, we first provided system design specifics encompassing from physical layer to higher layers. We then focused on the key technologies that can realize reliable and efficient mmWave-based high mobility support including beamforming, handover, and mobile relaying. We also presented the testbed implementation details for the gNodeB and UE. After describing the testbed deployment on the actual highway test track, we provided experimental results obtained in the field trial including SNR and data rate distributions, etc.

REFERENCES

[1] *Minimum Requirements Related to Technical Performance for IMT-2020 Radio Interface(S)*, ITU-R M.2410-0, Nov. 2017.

[2] *Study on Evaluation Methodology of New Vehicle-to-Everything V2X Use Cases for LTE and NR*, document 3GPP TR 37.885, Sep. 2018.

[3] *Study on Enhancement of 3GPP Support for 5G V2X Services*, 3GPP TR 22.886, V. 15.3.0, Sep. 2018.

[4] E. Dahlman, S. Parkvall, and J. Skold, *5G NR: The Next Generation Wireless Access Technology*. London, U.K.: Academic, 2018.

[5] H.-S. Park, Y. Lee, T.-J. Kim, B.-C. Kim, and J.-Y. Lee, "Handover mechanism in NR for ultra-reliable low-latency communications," *IEEE Netw.*, vol. 32, no. 2, pp. 41–47, Mar. 2018.

[6] *NR Mobility Enhancements*, document RP-192534, 3GPP, Dec. 2019.

[7] *Study on Scenarios and Requirements for Next Generation Access Technologies*, document 3GPP TR 38.913, V. 14.3.0, Jun. 2017.

[8] J. Wu and P. Fan, "A survey on high mobility wireless communications: Challenges, opportunities and solutions," *IEEE Access*, vol. 4, pp. 450–476, 2016.

[9] C. Madapatha, B. Makki, C. Fang, O. Teyeb, E. Dahlman, M.-S. Alouini, and T. Svensson, "On integrated access and backhaul networks: Current status and potentials," *IEEE Open J. Commun. Soc.*, vol. 1, pp. 1374–1389, Sep. 2020.

[10] M. Okano, Y. Hasegawa, K. Kanai, B. Wei, and J. Katton, "Field experiments of 28 GHz band 5G system at indoor train station platform," in *Proc. IEEE 17th Annu. Consum. Commun. Netw. Conf. (CCNC)*, Jan. 2020, pp. 1–6.

[11] L. Wu, D. He, K. Guan, B. Ai, J. Kim, and H. Chung, "Millimeter-wave channel characterization for vehicle-to-infrastructure communication," in *Proc. Eur. Conf. Ant. Prop. (EuCAP)*, Mar. 2020, pp. 1–5.

[12] K. Kim, M. Kim, J. Lee, J. Park, Y. K. Yoon, and Y. J. Chong, "Millimeter-wave diffraction-loss model based on over-rooftop propagation measurements," *ETRI J.*, vol. 42, no. 6, pp. 827–836, Dec. 2020.

[13] T. R. Dean, M. Chowdhury, N. Grimwood, and A. J. Goldsmith, "Rethinking modulation and detection for high Doppler channels," *IEEE Trans. Wireless Commun.*, vol. 19, no. 6, pp. 3629–3642, Jun. 2020.

[14] G. D. Surabhi, M. K. Ramachandran, and A. Chockalingam, "OTFS modulation with phase noise in mmWave communications," in *Proc. IEEE 89th Veh. Technol. Conf. (VTC-Spring)*, May 2019, pp. 1–5.

[15] N. Ishikawa, R. Rajashekar, C. Xu, M. El-Hajjar, S. Sugiura, L.-L. Yang, and L. Hanzo, "Differential-detection aided large-scale generalized spatial modulation is capable of operating in high-mobility millimeter-wave channels," *IEEE J. Sel. Topics Signal Process.*, vol. 13, no. 6, pp. 1360–1374, Oct. 2019.

[16] J. Rodriguez-Fernandez, N. Gonzalez-Prelcic, K. Venugopal, and R. W. Heath, Jr., "Exploiting common sparsity for frequency-domain wideband channel estimation at mmWave," in *Proc. IEEE Global Commun. Conf. (GLOBECOM)*, Dec. 2017, pp. 1–6.

[17] Q. Qin, L. Gui, P. Cheng, and B. Gong, "Time-varying channel estimation for millimeter wave multiuser MIMO systems," *IEEE Trans. Veh. Technol.*, vol. 67, no. 10, pp. 9435–9448, Oct. 2018.

[18] Q. Ma, G. Qiu, Q. Zhang, H. Sun, Z. Feng, and Z. Han, "Training sequence based Doppler shift estimation for vehicular communication," in *Proc. IEEE Wireless Commun. Netw. Conf. (WCNC)*, May 2020, pp. 1–6.

[19] J. Li, Y. Sun, L. Xiao, S. Zhou, and A. Sabharwal, "How to mobilize mmWave: A joint beam and channel tracking approach," in *Proc. IEEE Int. Conf. Acoust., Speech Signal Process. (ICASSP)*, Apr. 2018, pp. 3624–3628.

[20] H. Chung, J. Kang, H. Kim, Y. M. Park, and S. Kim, "Adaptive beamwidth control for mmWave beam tracking," *IEEE Commun. Lett.*, vol. 25, no. 1, pp. 137–141, Jan. 2021.

[21] M. Polese, M. Giordani, M. Mezzavilla, S. Rangan, and M. Zorzi, "Improved handover through dual connectivity in 5G mmWave mobile networks," *IEEE J. Sel. Areas Commun.*, vol. 35, no. 9, pp. 2069–2084, Sep. 2017.

[22] M. Mezzavilla, S. Goyal, S. Panwar, S. Rangan, and M. Zorzi, "An MDP model for optimal handover decisions in mmWave cellular networks," in *Proc. Eur. Conf. Netw. Commun. (EuCNC)*, Jun. 2016, pp. 100–105.

[23] *Study on New Radio Access Technology: Radio Access Architecture and Interfaces*, document 3GPP TR 38.801, V. 14.0.0, Mar. 2017.

[24] G. C. Valastro, D. Panno, and S. Riolo, "A SDN/NFV based C-RAN architecture for 5G mobile networks," in *Proc. Int. Conf. Sel. Topics Mobile Wireless Netw. (MoWNeT)*, Jun. 2018, pp. 1–8.

[25] G. Noh, H. Chung, and I. Kim, "Mobile relay technology for 5G," *IEEE Wireless Commun.*, vol. 27, no. 3, pp. 6–7, Jun. 2020.

[26] T. S. Rappaport, S. Sun, R. Mayzus, H. Zhao, Y. Azar, K. Wang, G. N. Wong, J. K. Schulz, M. Samimi, and F. Gutierrez, "Millimeter wave mobile communications for 5G cellular: It will work!" *IEEE Access*, vol. 1, pp. 335–345, 2013.

[27] J. Kim, G. Casati, N. Cassiau, A. Pietrabissa, A. Giuseppi, D. Yan, E. C. Strinati, M. Thary, D. He, K. Guan, and H. Chung, "Design of cellular, satellite, and integrated systems for 5G and beyond," *ETRI J.*, vol. 42, no. 5, pp. 669–688, Oct. 2020.

[28] K. Satyanarayana, T. Ivanescu, M. El-Hajjar, P.-H. Kuo, A. Mourad, and L. Hanzo, "Hybrid beamforming design for dual-polarised millimetre wave MIMO systems," *IET Elect. Lett.*, vol. 54, no. 22, pp. 1257–1258, Nov. 2018.

[29] *NR Physical Channels and Modulation*, document 3GPP TS 38.211, V. 16.3.0, Sep. 2020.

[30] *NR and NG-RAN Overall Description*, document 3GPP TS 38.300, V. 16.3.0, Sep. 2020.

[31] F. Jameel, S. Wyne, S. J. Nawaz, and Z. Chang, "Propagation channels for mmWave vehicular communications: State-of-the-art and future research directions," *IEEE Wireless Commun.*, vol. 26, no. 1, pp. 144–150, Feb. 2019.

[32] *Radio Resource Control (RRC) Protocol Specification*, document 3GPP TS 38.331, V. 16.0.0, Mar. 2020.

[33] K. D. C. Silva, Z. Becvar, and C. R. L. Frances, "Adaptive hysteresis margin based on fuzzy logic for handover in mobile networks with dense small cells," *IEEE Access*, vol. 6, pp. 17178–17189, 2018.

[34] J.-H. Choi and D.-J. Shin, "Generalized RACH-less handover for seamless mobility in 5G and beyond mobile networks," *IEEE Wireless Commun. Lett.*, vol. 8, no. 4, pp. 1264–1267, Aug. 2019.

[35] T. Li, H. Meng, and W. Dou, "Design and implementation of dual-frequency dual-polarization slotted waveguide antenna array for Ka-band application," *IEEE Antennas Wireless Propag. Lett.*, vol. 13, pp. 1317–1320, Jul. 2014.
[36] E. B. Basch, R. Egorov, S. Gringeri, and S. Elby, "Architectural tradeoffs for reconfigurable dense wavelength-division multiplexing systems," *IEEE J. Sel. Topics Quantum Electron.*, vol. 12, no. 4, pp. 615–626, Jul. 2006.

GOSAN NOH (Member, IEEE) received the B.S. and Ph.D. degrees in electrical and electronic engineering from Yonsei University, Seoul, South Korea, in 2007 and 2012, respectively. From March 2012 to February 2013, he was a Postdoctoral Researcher with the School of Electrical and Electronic Engineering, Yonsei University. Since March 2013, he has been with the Electronics and Telecommunications Research Institute (ETRI), Daejeon, South Korea, where he is currently a Senior Researcher. He has also been involved in 3GPP 5G NR standardization as ETRI's delegate of 3GPP RAN1 working group, since 2016. He has published more than 45 scientific papers in journals and conferences. He has contributed to several areas of telecommunications, including spectrum sharing, millimeter-wave transmission, and high mobility applications.

JUNHYEONG KIM (Member, IEEE) received the B.E. degree from the Department of Electronic Engineering, Tsinghua University, Beijing, China, in 2008, and the M.S. and Ph.D. degrees from the School of Electrical Engineering, Korea Advanced Institute of Science and Technology (KAIST), Daejeon, South Korea, in 2011 and 2020, respectively. Since 2011, he has been with the Electronics and Telecommunications Research Institute (ETRI), where he is taking part in the development of mmWave-band vehicular communication systems. He has been involved in the 5G New Radio standardization in the 3GPP RAN1 Working Group as a delegate at ETRI, since August 2017. His main research interests include mmWave communications, vehicular communications, cooperative communications, and handover.

SEUNGNAM CHOI received the B.S., M.S., and Ph.D. degrees in electronic engineering from Chonnam National University, Gwangju, South Korea, in 1998, 2000, and 2015, respectively. Since 2000, he has joined the Electronics and Telecommunications Research Institute (ETRI), Daejeon, South Korea, as a Principal Researcher. His research interests include 5G/6G mobile communications and millimeter-wave communications.

NAMSUK LEE received the M.S. degree in computer engineering and the Ph.D. degree in electrical and electronics engineering from Chungbuk National University, South Korea, in 2000 and 2010, respectively. He is currently a Principal Research with the Electronics and Telecommunication Research Institute (ETRI). His research interests include UE relay, V2X, sidelink, and handover.

HEESANG CHUNG received the bachelor's degree in physics from KAIST, South Korea, in 1993, and the Ph.D. degree in physics from Chungnam National University, South Korea, in 1999. He was involved in research projects on the optical communications, from 1999 to 2005. In 2005, he moved to the Wireless Communications Department, ETRI. Since 1999, he has been with the Electronics and Telecommunications Research Institute, South Korea. He had been involved in research projects on LTE and LTE-Advanced, from 2006 to 2010. His recent research interests include 5G and millimeter-wave based mobile communications, including mobile wireless backhauls for public transportation.

ILGYU KIM received the B.S. and M.S. degrees in electronics engineering from the University of Seoul, South Korea, in 1993 and 1995, respectively, and the Ph.D. degree in information communications engineering from KAIST, in 2009.

He worked with Shinsegi Telecom, from 1994 to 1999, where he took part in the optimization of IS-95 CDMA radio network and the international standardization of W-CDMA. Since 2000, he has been with the Electronics and Telecommunications Research Institute, where he involved in the standardization and development of WCDMA, HSPA, and LTE. He was in charge of the development of LTE UE modem chip set and MHN system. Since 2019, he has been an Assistant Vice President of ETRI and the Managing Director of the Future Mobile Communication Research Division. His current research interests include millimeter wave/THz communications and future mobile communications.